Gas-Phase Acidities and O−H Bond Dissociation Enthalpies of Phenol, 3-Methylphenol, 2,4,6-Trimethylphenol, and Ethanoic Acid

Laurence A. Angel and Kent M. Ervin*

Department of Chemistry and Chemical Physics Program, University of Nevada, Reno, 1664 North Virginia Street, Reno, Nevada 89557

Received: May 4, 2006; In Final Form: June 26, 2006

Energy-resolved, competitive threshold collision-induced dissociation (TCID) methods are used to measure the gas-phase acidities of phenol, 3-methylphenol, 2,4,6-trimethylphenol, and ethanoic acid relative to hydrogen cyanide, hydrogen sulfide, and the hydroperoxyl radical using guided ion beam tandem mass spectrometry. The gas-phase acidities of $\Delta_{acid}H_{298}(C_6H_5OH) = 1456 \pm 4$ kJ/mol, $\Delta_{acid}H_{298}(3\text{-}CH_3C_6H_4OH) = 1457 \pm 5$ kJ/mol, $\Delta_{acid}H_{298}(2,4,6\text{-}(CH_3)_3C_6H_2OH) = 1456 \pm 4$ kJ/mol, and $\Delta_{acid}H_{298}(CH_3COOH) = 1457 \pm 6$ kJ/mol are determined. The O−H bond dissociation enthalpy of $D_{298}(C_6H_5O-H) = 361 \pm 4$ kJ/mol is derived using the previously published experimental electron affinity for C_6H_5O, and thermochemical values for the other species are reported. A comparison of the new TCID values with both experimental and theoretical values from the literature is presented.

1. Introduction

Competitive threshold collision induced dissociation (TCID)[1] of a thermalized proton-bound $[X\cdots H\cdots Y]^-$ anionic complex enables a direct measurement of the relative gas-phase acidity between an unknown and a dissimilar reference acid.[2] The gas-phase acidity of a species is an important thermochemical property and is related to the bond dissociation enthalpy through the negative ion thermochemical cycle,[3] $D_0(X-H) = \Delta_{acid}H_0(XH) + EA_0(X) - IE_0(H)$. An extensive gas-phase acidity scale has been constructed from gas-phase ion−molecule equilibrium measurements.[4,5] An important anchor molecule in the gas-phase acidity scale is phenol.[6,7] However, there remains significant discrepancy in the literature from gas-phase experimental measurements,[7−23] photoacoustic calorimetry studies,[24−26] and evaluations[27−33] for the gas-phase acidity and O−H bond dissociation enthalpy of phenol. Theoretical calculations of the bond dissociation enthalpy also do not converge on a single value.[23,33−46]

A debate over the correct value of the O−H bond dissociation enthalpy of phenol has appeared in the literature recently.[33,44−46] Recently, we reported the bond dissociation of $D_{298}(C_6H_5O-H) = 359 \pm 8$ kJ/mol for phenol using the TCID method with the single reference acid HCN.[23] The $D_{298}(C_6H_5O-H) = 359 \pm 8$ kJ/mol value is significantly lower than other recently cited experimental values in the literature,[18,20,22] including one from this laboratory.[21] Ervin and DeTuri previously used a proton-transfer reaction between $Cl^- + C_6H_5OH$ in a guided ion beam experiment (PT/GIB) to determine $D_{298}(C_6H_5O-H) = 377 \pm 13$ kJ/mol.[21] However, in a subsequent study of similar bimolecular proton-transfer reactions, the threshold energies were found to systematically exceed the expected values by 5−9 kJ/mol.[47] Better results were obtained by assuming that rotational energy is not available to promote reaction. This issue of the role rotational energy in bimolecular proton-transfer reactions remains unresolved, but the threshold value should be treated as an upper limit, $D_{298}(C_6H_5O-H) \leq 377 \pm 13$ kJ/mol.

The more recently developed competitive TCID method[1,2,48] overcomes the problems associated with the bimolecular proton-transfer reactions. Our group reported TCID measurements on proton-bound complexes of a series of alcohols using guided ion beam mass spectrometry techniques.[2,49] The results from TCID were in excellent agreement with previously established literature values and provided absolute acidities within ±4 kJ/mol. Because of the proven accuracy of the TCID method, we were confident of our recent $D_{298}(C_6H_5O-H) = 359 \pm 8$ kJ/mol value, but did not anticipate that a single new measurement would settle the controversy regarding the bond dissociation enthalpy of phenol. This paper presents many additional TCID measurements, and the construction of a thermochemical ladder in the region of the gas-phase acidity scale of phenol with the additional acids of 3-methylphenol, 2,4,6-trimethylphenol, ethanoic acid (acetic acid), hydrogen cyanide, hydrogen sulfide, and the hydroperoxyl radical. A gas-phase acidity ladder with interlocking measurements will allow the determination of an absolute $\Delta_{acid}H_0(C_6H_5OH)$ and a derived $D_{298}(C_6H_5O-H)$ value with higher precision than those obtained previously.

2. Experimental Methods

2.1. Threshold Collision-Induced Dissociation. A thermalized proton-bound $[X\cdots H\cdots Y]^-$ anionic complex is collisionally excited at a controlled translational energy, resulting in the two dissociation products, as shown in reaction 1.

$$[X\cdots H\cdots Y]^- + Xe \rightarrow X^- + HY + Xe \quad (1a)$$

$$\rightarrow XH + Y^- + Xe \quad (1b)$$

The energy threshold difference between the two reaction channels in reaction 1 is related to the gas-phase acidities of

* Corresponding author. E-mail: ervin@chem.unr.edu.

10.1021/jp0627426 CCC: $33.50
Published on Web 08/17/2006

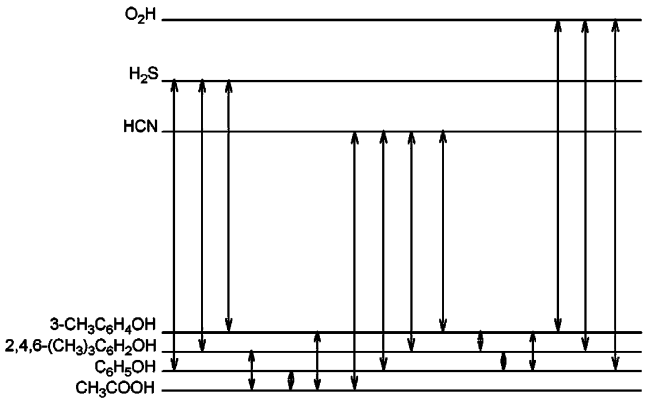

Figure 1. Local thermochemical network (not exactly to scale). Arrows show the 16 combinations of measured gas-phase acidity differences between the species.

TABLE 1: Thermochemical Values

thermochemical property	value/(kJ/mol)	ref
$EA_0(CN)$	372.6 ± 0.4	50
$D_0(H-CN)$	522.9 ± 0.8	51
$IE_0(H)$	1312.049 ± 0.001	52
$\Delta_{acid}H_0(HCN)$	1462.3 ± 0.9	a
$EA_0(O_2)$	43.2 ± 0.6	53
$D_0(H-O_2)$	199.2 ± 3.3	54
$\Delta_fH_0(OOH)$	16.3 ± 2.1	55
$\Delta_{acid}H_0(HO_2)$	1468.6 ± 2.2	b
$\Delta_{acid}H_0(H_2S)$	1464.92 ± 0.04	56
$\Delta_fH_{298}(C_6H_5OH)$	-96.4 ± 0.9	57
$\Delta_fH_{298}(3\text{-}CH_3C_6H_4OH)$	-133.6 ± 1.1	58, 59
$\Delta_fH_{298}(2,4,6\text{-}(CH_3)_3C_6H_2OH)$	-176.9 ± 2.0	58
$\Delta_fH_{298}(CH_3COOH)$	-432.1 ± 0.4	60
$\Delta_fH_{298}(H)$	217.998 ± 0.006	52
$EA_0(C_6H_5O)$	217.38 ± 0.58	19
$EA_0(CH_3COO)$	334.8 ± 1.0	61

[a] $\Delta_{acid}H_0(RH) = D(R-H) - EA(R) + IE(H)$. [b] $\Delta_{acid}H_0(OOH)$ derived from $\Delta_fH_0(OOH)$.

XH and HY by eq 2.

$$\Delta E_0 = E_0(1b) - E_0(1a) = \delta\Delta_{acid}H_0 \quad (2a)$$

$$\delta\Delta_{acid}H_0 = \Delta_rH_0(1b) - \Delta_rH_0(1a) = \Delta_{acid}H_0(HY) - \Delta_{acid}H_0(XH) \quad (2b)$$

The equality on the right-hand side of eq 2a holds if there are no reverse activation barriers or dynamical constrictions for the two dissociation channels. To extract the two threshold energies, the energy-dependent branching ratio between the two channels is modeled explicitly using RRKM theory.[1,2,48] To construct a local thermochemical network, the relative acidities of sixteen combinations of seven chemical species are measured and anchored to the well-defined reference acids of HCN, OOH, and H_2S. The local thermochemical network is illustrated in Figure 1. The previously established thermochemical data for HCN, OOH, and H_2S are shown in Table 1.[19,49-61] To derive the RO−H bond dissociation enthalpy, we use the precisely known ionization energy (IE) of the hydrogen atom and the electron affinity (EA) of the RO radical. An accurate electron affinity of the phenoxy radical has been obtained by negative ion photoelectron spectroscopy.[19] The photoelectron spectrum of $C_6H_5O^-$ has a well-resolved origin transition, giving a clear assignment of the electron affinity.[19]

2.2. Cross-Section Measurements. Experiments were carried out using our guided ion beam tandem mass spectrometer, which has been previously described in detail.[62,63] The thermalized $[X\cdots H\cdots Y]^-$ complexes, where X and Y are one of CN, HS, O_2, C_6H_5O, $3\text{-}CH_3C_6H_4O$, $2,4,6\text{-}(CH_3)_3C_6H_2O$, or CH_3COO, are formed in a flow tube reactor by producing Y^- anions in a microwave discharge and adding XH downstream of the microwave discharge. A magnetic sector mass spectrometer is used to select the complexes before they are injected into an octopole ion beam guide, where they collide with xenon atoms at a controlled translational energy. Reactant and product ions are extracted from the octopole region, mass analyzed with a quadrupole mass filter, and counted using a conversion dynode/channeltron multiplier operated in negative-ion counting mode.

Absolute reaction cross-sections are determined as a function of collision energy between the reactants; a thorough discussion has been presented previously.[62,64] The origin of the laboratory ion energy is measured before and after each scan by retarding potential analysis and checked daily by a time-of-flight measurement.[62] The laboratory ion energy is then converted to the relative collision energy, E, in the center-of-mass frame.[64] To obtain absolute reaction cross-sections under single-collision conditions, the data are collected at three different pressures and the cross-sections are extrapolated to zero pressure. The absolute cross-section magnitudes have an estimated uncertainty of ±50%, but for two product channels the relative values should be within ±10%.

2.3. Cross-Section Modeling. Details of the cross-section modeling have been discussed in detail previously,[23] including the relative collision energy, E, and the angular momentum quantum number, J, distributions for competitive threshold collision-induced dissociation and treatment of angular momentum effects.[1,2,48] The analysis is implemented using the CRUNCH program.[65] Briefly, the reaction cross-sections for both products are modeled simultaneously using RRKM theory[66,67] to obtain the energy difference between the two channels. The transition states may be treated as fixed (tight) or orbiting (loose, i.e., located at the centrifugal barrier).[66,67] The long-range potential is calculated for the ion-induced-dipole interaction with the neutral molecule permanent dipole treated either in a zero-dipole approximation[48] or in a locked-dipole approximation,[68] using the molecular polarizability[69] and dipole moment[70] of the neutral product. CRUNCH also allows use of a transition-state (TS) switching model.[71] The transition-state switching model uses both an outer loose transition state and an inner tight transition state to fit the experimental data. At a given collision energy, the TS with the lowest sum of states is considered the restricting TS and is used to calculate the rate constant k_j. The total internal energy of the complex E^* is given by its initial thermal energy from the ion source plus the energy ϵ transferred upon collision, using the empirical distribution function in eq 3,[72]

$$P_e(\epsilon,E) = \sigma_0 N \frac{(E-\epsilon)^{N-1}}{E} \quad (3)$$

where E is the relative collision energy in the center-of-mass frame, σ_0 is a scaling factor related to the total collision cross-section, and N is an adjustable parameter that describes the efficiency of translational-to-internal energy transfer. The probability of dissociation and detection of the energized complex to product channel j is given by first-order reaction kinetics with parallel product channels, as described by eq 4,

$$P_{D,j}(E^*,J) = \frac{k_j(E^*,J)}{k_{tot.}(E^*,J)}[1 - \exp(-k_{tot.}(E^*,J))\tau] \quad (4)$$

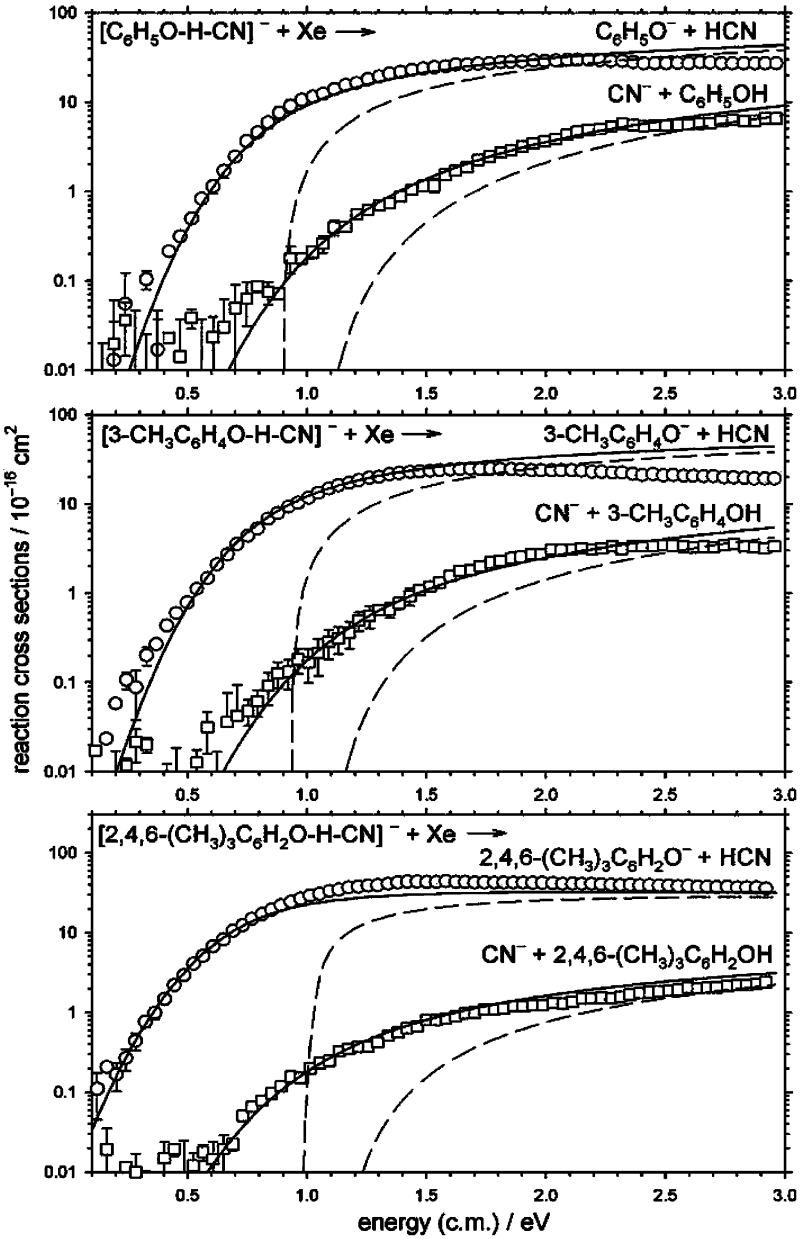

Figure 2. Single-collision TCID cross sections for $[RO-H-CN]^- \rightarrow RO^- + HCN$, $CN^- + ROH$ as a function of relative collision energy between $[RO-H-CN]^-$ and Xe. Solid lines show the convoluted fits to the data and dashed lines the corresponding unconvoluted 0 K model cross-sections.

where $k_{tot.} = \Sigma k_j$ is the total dissociation rate constant of the individual channels j and τ is the time-of-flight of the center-of-mass of the system from the collision cell to the mass spectrometer detector. J is the angular momentum quantum number for the rotational energies of the energized molecule and transition-state configuration for the 2-D pseudolinear rotor comprising the two fragments. To model experimental cross-sections, eq 4 is integrated over (a) the Boltzmann distribution of initial internal energies of the proton-bound complex, (b) the distribution of energy collisionally transferred,[72] (c) the angular momentum distribution in a statistical approximation,[2,48] (d) the Maxwell−Boltzmann thermal velocity distribution of the target gas,[73] and (e) a Gaussian distribution of ion beam kinetic energies with the measured full-width at half-maximum.[64,74] The final model cross-sections are fit to both product channels simultaneously by a nonlinear least-squares optimization to obtain $E_0(1)$ and ΔE_0 along with σ_0 and N as adjustable parameters.[1]

3. Results

3.1. Cross-Sections and Threshold Analysis. The cross-sections for $X^- + HY$ and $Y^- + XH$ products from the dissociation of the $[X-H-Y]^-$ complexes are shown in Figures 2−6. Solid lines in the figures show the convoluted fits to the data, while the dashed lines show the 0 K unconvoluted model cross-sections (without the translational or internal energy distributions but including the RRKM branching ratio and kinetic shift). The energy range used to fit the experimental data is chosen to reproduce as much of the experimental cross-section data as possible while maintaining a good fit in the threshold region. The best fits were achieved by using energy ranges within 0.1−3.0 eV. It is expected that the statistical rate approximation and density of states calculations are less reliable at higher energies than near threshold. Table 2 lists the results of the empirical fits for both the zero-dipole and locked-dipole approximations for the permanent dipole, where $E_0(1) = \Delta_c H_0$

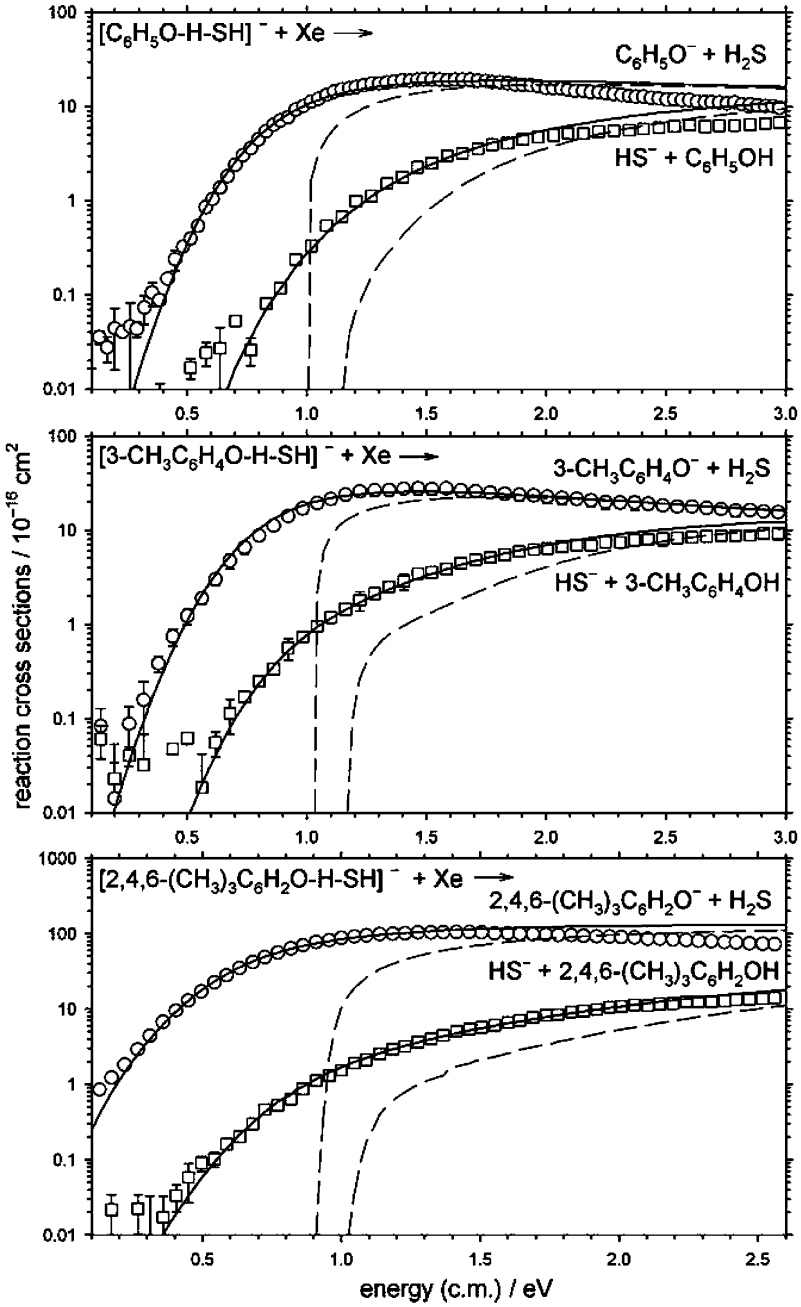

Figure 3. Single-collision TCID cross-sections for $[RO{-}H{-}SH]^- \rightarrow RO^- + H_2S$, $HS^- + ROH$ as a function of relative collision energy between $[RO{-}H{-}SH]^-$ and Xe. Solid lines show the convoluted fits to the data and dashed lines the corresponding unconvoluted 0 K model cross-sections.

is the dissociation threshold energy for the lower-energy channel and is equal to the complex dissociation energy of $[X\cdots HY]^-$, and $\Delta E_0 = E_0(2) - E_0(1)$ is the energy difference between the two reaction channels.

3.2. RRKM Transition-State Models. A loose, orbiting transition-state model[48,66,67] was found to satisfactorily fit the experimental cross-sections for all the complexes shown in Table 2, except for the complexes that have a channel leading to the formation of H_2S, for which fits using the loose TS model were poor (shown in Figure S1). The loose, orbiting transition-state model is usually appropriate because the complex is held together by electrostatic forces and hydrogen bonding, rather than a covalent bond. For the cases where a channel leads to the formation of H_2S, however, the cross-sections could only be satisfactorily fit by using the transition-state switching model.[71] For the $RO^- + H_2S$ channel, the loose TS is the restricting TS near the threshold but the tight TS becomes restricting only at slightly higher energies that are still in the region of the rising cross-sections.

The error bars quoted in Table 2 are the root-sum-of-squares from individual sources of uncertainty (assuming they are independent of each other) and represent estimates of ± 2 combined standard uncertainties.[75] Uncertainties were included from the ion beam energy zero determination ± 0.05 eV (laboratory), from the statistical uncertainty in the least-squares fit to the data, from the standard deviation of data taken on separate occasions, from the consistency of the model fit using different energy ranges, and by varying the model parameters used to fit the TCID data by $\pm 10\%$.

3.3. Molecular Orbital Calculations. Representative potential energy surfaces (PES), for $[C_6H_5O{-}H{-}SH]^-$ and $[C_6H_5O{-}H{-}OOCCH_3]^-$, calculated at B3LYP/aug-cc-pVDZ using Gauss-

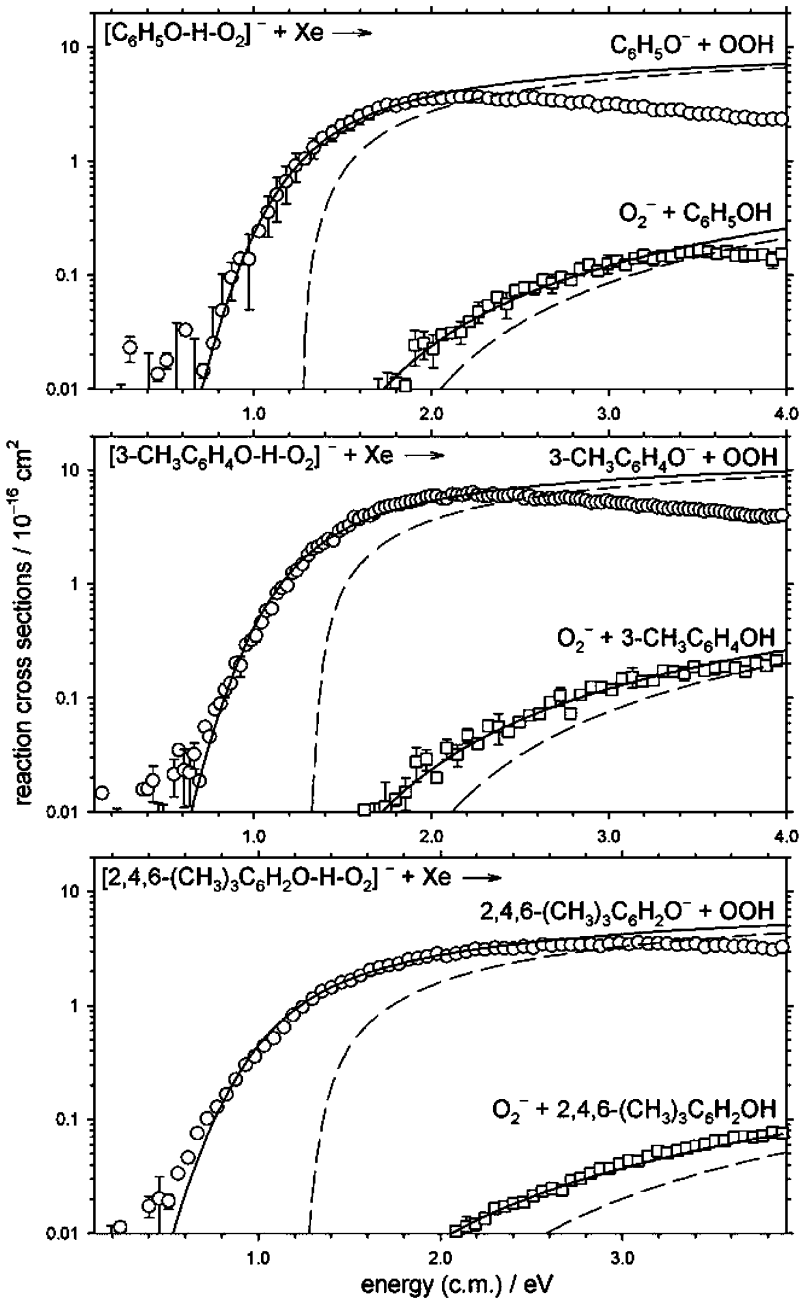

Figure 4. Single-collision TCID cross-sections for $[RO{-}H{-}O_2]^- \rightarrow RO^- + HOO$, $O_2^- + ROH$ as a function of relative collision energy between $[RO{-}H{-}O_2]^-$ and Xe. Solid lines show the convoluted fits to the data and dashed lines the corresponding unconvoluted 0 K model cross-sections.

ian 03[76] are shown in Figure 7. Both PESs exhibit a deep well associated with the formation of the complex and two steep repulsive surfaces out to the product channels. There are no reverse potential energy barriers separating the products from the complex. An illustration showing the structure of the lowest energy complex, where the proton is associated with the phenol, is included in Figure 7. Along the exit surfaces out to the $C_6H_5O^- + H_2S$ and $C_6H_5O^- + CH_3COOH$ products both PESs exhibit small inflection points between −70 and −60 kJ/mol and −110 and −100 kJ/mol, respectively, where the proton transfers from C_6H_5OH to either HS^- or CH_3COO^-. The PES for $[C_6H_5O{\cdot}H{\cdot}CN]^-$ at the B3LYP/aug-cc-pVDZ level of theory has been previously published.[23] These surfaces are representative of the results for complexes of HS^-, CN^-, and CH_3COO^- with $3\text{-}CH_3C_6H_4OH$ and $2,4,6\text{-}(CH_3)_3C_6H_2OH$. The PES for $[C_6H_5O{-}H{-}O_2]^-$, which has a doublet ground state, exhibited high spin contamination resulting in the electron charge being distributed between the products, however, so these calculations could not be satisfactorily completed at this level of theory.

Molecular parameters of the complexes and products for the RRKM modeling are either taken from the literature or computed at the B3LYP/aug-cc-pVDZ or HF/6-31G(d) levels of theory and are listed in the supporting material Table S1. Torsional motions around the C−O axis are treated as hindered rotors for C_6H_5OH, $3\text{-}CH_3C_6H_4OH$, $2,4,6\text{-}(CH_3)_3C_6H_2OH$, CH_3COOH, $[C_6H_5O{-}H{-}CN]^-$, $[C_6H_5O{-}H{-}SH]^-$, $[C_6H_5O{-}H{-}O_2]^-$,$[3\text{-}CH_3C_6H_4O{-}H{-}CN]^-$,$[3\text{-}CH_3C_6H_4O{-}H{-}SH]^-$,$[3\text{-}CH_3C_6H_4O{-}H{-}O_2]^-$, $[2,4,6\text{-}(CH_3)_3C_6H_2O{-}H{-}CN]^-$, $[2,4,6\text{-}(CH_3)_3C_6H_2O{-}H{-}SH]^-$, and $[2,4,6\text{-}(CH_3)_3C_6H_2O{-}H{-}O_2]^-$ using methods presented previously.[2,23]

3.4. Gas-Phase Acidity Determination. The absolute gas-phase acidities of the alcohols are determined by a least-squares

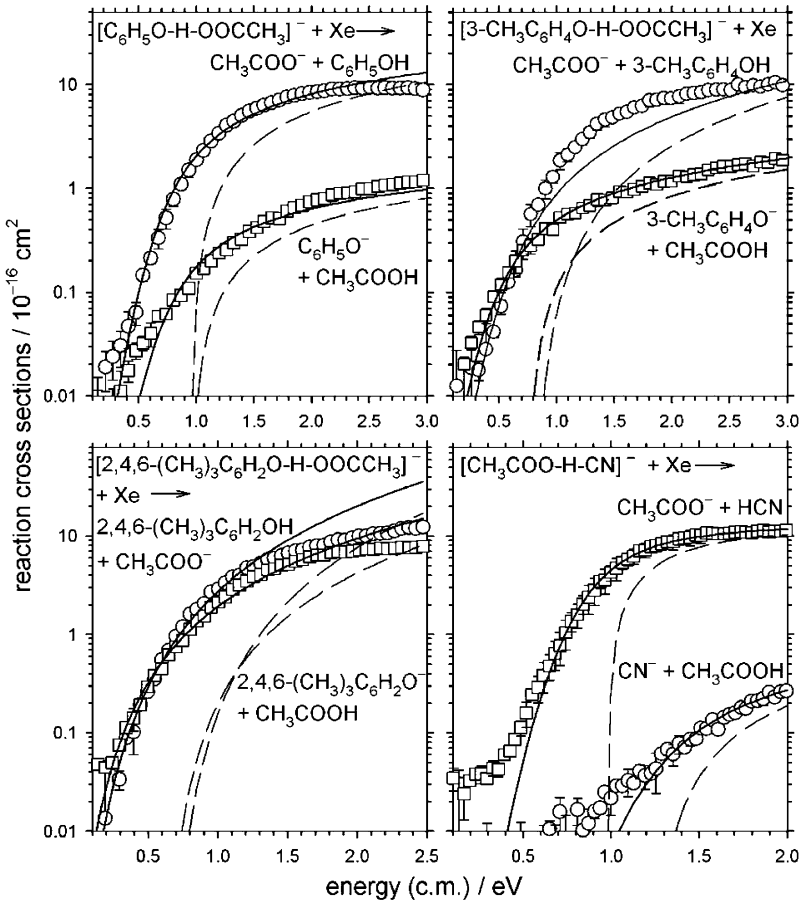

Figure 5. Single-collision TCID cross-sections for $[X-H-OOCCH_3]^- \rightarrow X^- + CH_3COOH$, $CH_3COO^- + XH$ as a function of relative collision energy between $[X-H-OOCCH_3]^-$ and Xe. Solid lines show the convoluted fits to the data and dashed lines the corresponding unconvoluted 0 K model cross-sections.

minimization of χ^2 from eq 5,

$$\chi^2 = \sum_{j\neq k}\left(\frac{\Delta_{acid}H_0(A_jH) - \Delta_{acid}H_0(A_kH) - \Delta E_0(j,k)}{\sigma_{j,k}}\right)^2 \Bigg/ \sum_{j\neq k}\left(\frac{1}{\sigma_{j,k}^2}\right) \quad (5)$$

where $\Delta E_0(j,k) = E_0(j) - E_0(k)$ is the measured gas-phase acidity difference for the complex $[A_kHA_j]^-$, $\Delta_{acid}H_0(A_jH)$ and $\Delta_{acid}H_0(A_kH)$ are the absolute gas-phase acidities, and $\sigma_{j,k}$ is the uncertainty in the relative gas-phase acidity measurement. The gas-phase acidities of hydrogen sulfide, hydrogen cyanide, and the hydroperoxyl radical are treated as constants (Table 1), and the gas-phase acidities of phenol, 3-methylphenol, 2,4,6-trimethylphenol, and ethanoic acid are the adjustable parameters. The $\Delta E_0(j,k)$ values are the experimental threshold energy differences for 48 independent measurements of 16 different complexes, with average values and the number of individual measurements for each complex listed in Table 2. The number of measurements involving each species in one product channel is $v = 21$ for C_6H_5OH, $v = 19$ for 3-$CH_3C_6H_4OH$, $v = 16$ for 2,4,6-$(CH_3)_3C_6H_2OH$, and $v = 10$ for CH_3COOH. The 95% confidence limits are calculated by either using the square roots of the diagonal elements of the covariance matrix as described by Ruscic et al.,[77] or by eq 6, where $n = 48$ is the number of measurements, $m = 4$ is the number of adjustable parameters, and t_{95} is the Student *t*-factor.[78]

$$\pm\delta_j = \pm t_{95}\sigma_j = \pm t_{95}\left[\left(\frac{n}{n-m}\right)\chi^2\right]^{1/2} \quad (6)$$

The covariance matrix method propagates the uncertainties from the individual measurements involving each species, while eq 6 accounts for the self-consistency of the gas-phase acidity ladder. Our final uncertainties are derived from the greater uncertainty of the two methods described above and propagated with the uncertainties associated with the literature gas-phase acidities of HCN, O_2H, and H_2S (Table 1). Table 3 shows the $\Delta_{acid}H_0$ results from the optimization by eq 5 from both the zero-dipole and locked-dipole approximations. Both dipole approximations give final $\Delta_{acid}H_0$ values that agree to within 1.3 kJ/mol. The locked-dipole approximation, however, exhibits a greater internal consistency in the final gas-phase acidity ladder when compared to the zero-dipole approximation, as shown by a smaller χ^2 by a factor of 3.4.

3.5. Thermochemical Derivations. Thermochemical values derived from the present work are summarized in Table 4. The final recommended $\Delta_{acid}H_0$ values are those from the locked-dipole approximation. The values for $\Delta_{acid}H_{298}$, $\Delta_{acid}G_{298}$, D_{298}-(RO−H), and Δ_fH_{298}(RO) are then derived from $\Delta_{acid}H_0$ using literature thermochemical values from Table 1 and statistical mechanics thermal corrections using molecular parameters given in the Supporting Information. The final uncertainties shown in Table 4 include an additional 0.5 kJ/mol uncertainty for con-

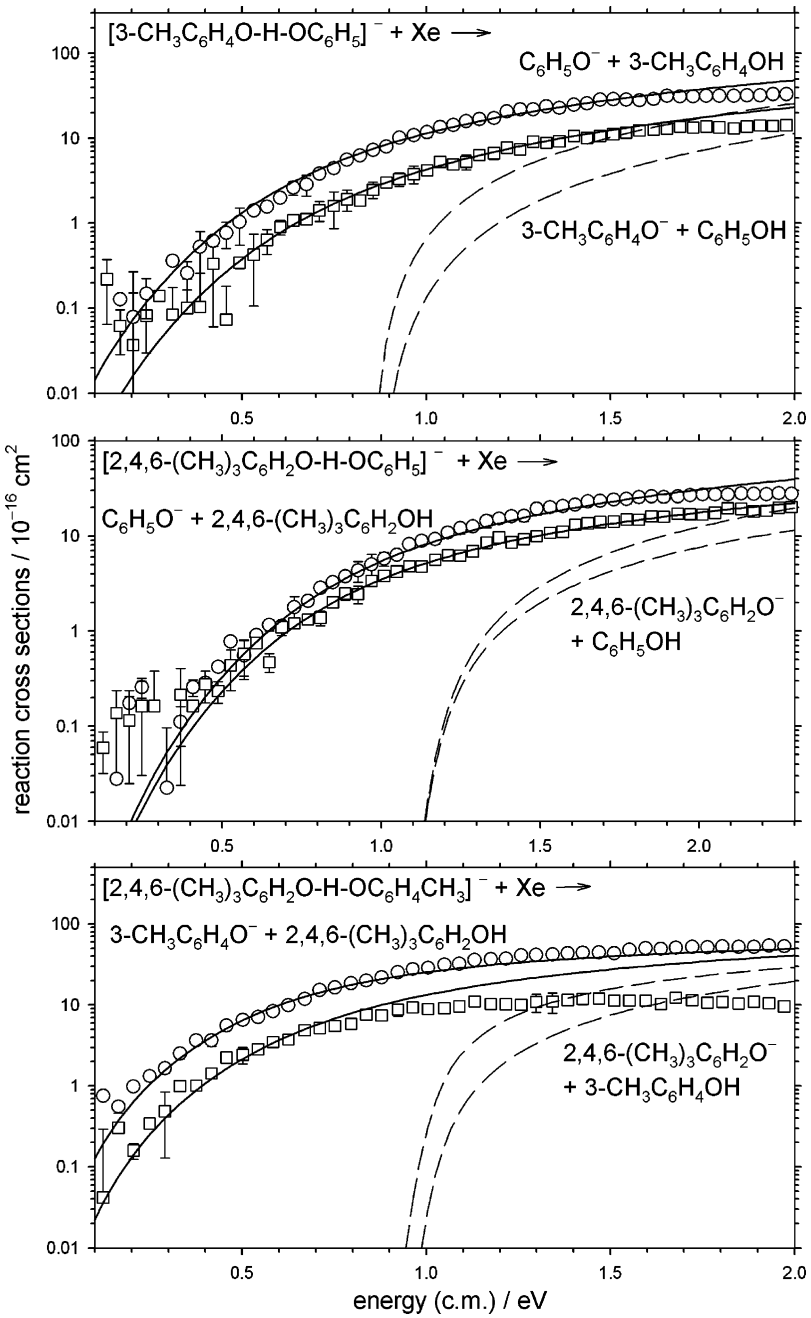

Figure 6. Single-collision TCID cross-sections for $[X-H-Y]- \rightarrow X^- + HY$, $Y^- + XH$ as a function of relative collision energy between $[X-H-Y]^-$ and Xe. Solid lines show the convoluted fits to the data and dashed lines the corresponding unconvoluted 0 K model cross-sections.

version from 0 to 298 K and are propagated with the uncertainties associated with the literature values shown in Table 1.

4. Discussion

4.1. Consistency in Gas-Phase Acidity Ladder. The greater consistency in the gas-phase acidity ladder from the locked-dipole approximation is shown by the smaller χ^2 value compared to the ion-induced dipole method in Table 3. The consistency improves again when all the individual measurements from the $[RO-H-SH]^-$ complexes are excluded from either of the dipole models. The improvement in consistency is because the individual ΔE_0 values from the $[RO-H-SH]^-$ complexes, summarized in Table 2, are systematically smaller in magnitude compared with expected values based on the ΔE_0 values from the $[RO-H-CN]^-$ and $[RO-H-O_2]^-$ complexes and the accepted acidities of H_2S, HCN, and HO_2. The offset of ΔE_0 values for $[RO-H-SH]^-$ is more pronounced with the zero-dipole approximation. The inclusion of the $[RO-H-SH]^-$ data to the optimization by eq 5 results in an increase to the $\Delta_{acid}H_0$ values shown in Table 3 of 2.8−4.1 kJ/mol when the zero-dipole ΔE_0 values are used but only 1.3−2.0 kJ/mol when the locked-dipole ΔE_0 values are used. Statistically, however, the $[RO-H-SH]^-$ data cannot be treated as outliers. A comparison of the internal consistency of the two dipole models can be further evaluated by using only two of the $\Delta_{acid}H_0$ anchor species as constant values with the third $\Delta_{acid}H_0$ value optimized as an additional unknown. If the gas-phase acidity of H_2S is treated as an additional unknown, eq 5 gives $\Delta_{acid}H_0(H_2S) = 1456.5 \pm 3.6$ kJ/mol for the zero-dipole method and $\Delta_{acid}H_0(H_2S) = 1461.2 \pm 3.7$ kJ/mol with the locked-dipole model. The zero-dipole value of $\Delta_{acid}H_0(H_2S) = 1456.5 \pm 3.6$ kJ/mol is outside the mutual error bars when compared to the $\Delta_{acid}H_0(H_2S) =$

TABLE 2: Threshold Fitting

complex [X−H−Y]⁻	zero dipole $E_0(1)$ (eV)	zero dipole ΔE_0 (eV)	locked dipole $E_0(1)$ (eV)	locked dipole ΔE_0 (eV)	data sets
$[C_6H_5O-H-CN]^-$	0.83 ± 0.15	0.164 ± 0.083	0.86 ± 0.15	0.128 ± 0.081	3
$[3\text{-}CH_3C_6H_4O-H-CN]^-$	0.91 ± 0.16	0.166 ± 0.082	0.95 ± 0.20	0.136 ± 0.087	3
$[2,4,6\text{-}(CH_3)_3C_6H_2O-H-CN]^-$	0.90 ± 0.26	0.159 ± 0.093	0.92 ± 0.28	0.133 ± 0.103	2
$[C_6H_5O-H-SH]^-$	0.99 ± 0.18	0.104 ± 0.095	1.01 ± 0.16	0.116 ± 0.094	3
$[3\text{-}CH_3C_6H_4O-H-SH]^-$	0.93 ± 0.24	0.089 ± 0.094	0.96 ± 0.26	0.111 ± 0.094	6
$[2,4,6\text{-}(CH_3)_3C_6H_2O-H-SH]^-$	0.90 ± 0.16	0.104 ± 0.104	0.91 ± 0.13	0.132 ± 0.104	4
$[C_6H_5O-H-O_2]^-$	1.30 ± 0.33	0.216 ± 0.094	1.29 ± 0.21	0.187 ± 0.093	3
$[3\text{-}CH_3C_6H_4O-H-O_2]^-$	1.30 ± 0.24	0.209 ± 0.094	1.33 ± 0.26	0.192 ± 0.094	2
$[2,4,6\text{-}(CH_3)_3C_6H_2O-H-O_2]^-$	1.11 ± 0.14	0.204 ± 0.095	1.16 ± 0.16	0.185 ± 0.095	2
$[C_6H_5O-H-OC_6H_4CH_3]^-$	0.90 ± 0.29	0.022 ± 0.100	0.91 ± 0.29	0.024 ± 0.100	4
$[C_6H_5O-H-OC_6H_2(CH_3)_3]^-$	0.84 ± 0.39	0.004 ± 0.120	0.94 ± 0.37	0.003 ± 0.120	4
$[3\text{-}CH_3C_6H_4O-H-OC_6H_2(CH_3)_3]^-$	0.86 ± 0.50	0.022 ± 0.140	0.83 ± 0.50	0.022 ± 0.140	2
$[CH_3COO-H-OC_6H_5]^-$	0.97 ± 0.30	0.005 ± 0.120	0.98 ± 0.30	0.011 ± 0.120	4
$[3\text{-}CH_3C_6H_4O-H-OOCCH_3]^-$	0.88 ± 0.28	0.027 ± 0.120	0.82 ± 0.27	0.022 ± 0.120	2
$[2,4,6\text{-}(CH_3)_3C_6H_2O-H-OOCCH_3]^-$	0.66 ± 0.38	0.021 ± 0.140	0.77 ± 0.45	0.012 ± 0.140	2
$[CH_3COO-H-CN]^-$	0.96 ± 0.43	0.199 ± 0.150	1.06 ± 0.35	0.172 ± 0.150	2

TABLE 3: Preliminary Thermochemical Results (0 K, kJ/mol)

species	zero dipole $\Delta_{acid}H_0$ [a]	zero dipole $\Delta_{acid}H_0$ [b]	locked dipole $\Delta_{acid}H_0$ [a,c]	locked dipole $\Delta_{acid}H_0$ [b]
C_6H_5OH	1449.7 ± 2.5 (6.0)[d]	1446.7 ± 3.0 (2.8)	1451.0 ± 2.5 (3.3)	1449.6 ± 3.0 (3.0)
$3\text{-}CH_3C_6H_4O$	1451.3 ± 2.4 (9.0)	1447.2 ± 3.3 (3.8)	1451.8 ± 2.4 (5.3)	1449.8 ± 3.3 (3.9)
$2,4,6\text{-}(CH_3)_3C_6H_2OH$	1450.8 ± 2.9 (6.7)	1447.5 ± 3.7 (3.2)	1451.3 ± 3.0 (3.0)	1450.0 ± 3.9 (2.7)
CH_3COOH	1450.1 ± 4.3 (7.8)	1447.3 ± 4.5 (5.4)	1450.6 ± 4.3 (6.4)	1449.3 ± 4.5 (5.4)
χ^2	13.8[e]	2.1	4.1	2.1

[a] H_2S, HCN and HOO used as anchors. [b] H_2S data removed; HCN and HOO used as anchors. [c] Recommended values (see text). [d] 95% confidence limits calculated using the covariance matrix[77] and in the parentheses by eq 6. [e] χ^2 value from eq 5.

1464.92 ± 0.04 kJ/mol value determined by Hepburn and coworkers.[56] The locked-dipole value of $\Delta_{acid}H_0(H_2S) = 1461.2 \pm 3.7$ kJ/mol, however, has overlapping mutual uncertainties with the literature value. Moreover, when either $\Delta_{acid}H_0$(HCN) or $\Delta_{acid}H_0$(OOH) is treated as unknown, there is much better agreement with their literature values when the locked-dipole method is used. In our previous work on phenol with the single reference species of hydrogen cyanide,[23] we simply averaged the zero-dipole and locked-dipole results (because both are approximations) but the significantly greater self-consistency found here for the locked-dipole method leads us to favor it.

The remaining small discrepancy for the $[RO-H-SH]^-$ systems could be due to nonstatistical reaction dynamics or problems in the RRKM modeling procedure using a transition-state switching model. For instance, there is a greater uncertainty involved in allocating the correct vibrational and rotational constants for the tight transition state for the $RO^- + H_2S$ products. Of all the systems studied, only the three $[RO-H-SH]^-$ systems needed the transition-state switching model to satisfactorily fit the rising cross-sections from the threshold region. The transition-state switching model is always needed for the dissociation channel that results in $RO^- + H_2S$ formation. The PES, shown in Figure 7, does not exhibit a barrier along the dissociation coordinate, but only a very small inflection between −70 and −80 kJ/mol separating the $[C_6H_5O-H-SH]^-$ complex and $H_2S + C_6H_5O^-$ products. This inflection point is the result of proton transfer from C_6H_5OH to HS^- within the complex. The requirement for proton transfer and the resulting high curvature along the reaction path, therefore, could be a possible dynamical impediment for the $RO^- + H_2S$ dissociation channel. Similar behavior has been previously observed from the reaction cross-sections and PES for the dissociation of the $[HS-H-CN]^-$ complex.[79] A dynamically restricted $H_2S + RO^-$ channel would explain the offset of the ΔE_0 values for the $[RO-H-SH]^-$ complexes when compared to the ΔE_0 values from $[RO-H-O_2]^-$ and $[RO-H-CN]^-$. Figure 7 shows that the PES for $[C_6H_5O-H-OOCH_3]^-$ also exhibits an inflection point at energies between −110 and −100 kJ/mol. However, the inflection point is just above the relative electronic energy of the $[C_6H_5O-H-OOCH_3]^-$ complex, and the inclusion of zero point energy will probably make the feature insignificant for the dissociation process out to products. Similar behavior has been previously observed for the dissociation of $[C_6H_5O-H-CN]^-$.[23]

The $C_6H_5O^- + OOH$ channel from the dissociation of the $[C_6H_5O-H-O_2]^-$ complex, shown in Figure 4, could also be fitted using a transition-state switching model. However, unlike the $[RO-H-SH]^-$ complexes, for $[C_6H_5O-H-O_2]^-$ the inclusion of a tight TS only improves the fitting at high collision energies, well above the threshold region. Moreover, the ΔE_0 values from using a transition-state switching model are identical to the ΔE_0 values obtained by modeling the $RO^- + OOH$ channel with a loose TS model. The $[RO-H-O_2]^-$ ΔE_0 values shown in Tables 2 and Figure 4 are from cross-section fits from the loose/loose TS model.

4.2. Comparison with Literature Experiments. A comparison of our TCID results with the NIST recommended values from proton-transfer equilibrium experiments is shown in Table 5.[7,10,58,80,81] Overall, there is reasonable agreement within the uncertainties between all the $\Delta_{acid}H_{298}$ values with $\Delta_{acid}H_{298}(CH_3COOH)$ agreeing the best. However, our TCID $\Delta_{acid}H_{298}$ results show a systematic lower offset of 2−6 kJ/mol when compared with the ion cyclotron resonance mass spectrometry (ICR) results and are lower by 2−10 kJ/mol when compared to the high-pressure mass spectrometry (HPMS) measurements. Our lower values may be partly attributed to the anchor systems used in the different experiments. For the ICR equilibrium studies, phenol, 3-methylphenol, and ethanoic acid are measured relative to each other or several acids with close-lying acidities and anchored to the gas-phase acidity of phenol, which in turn

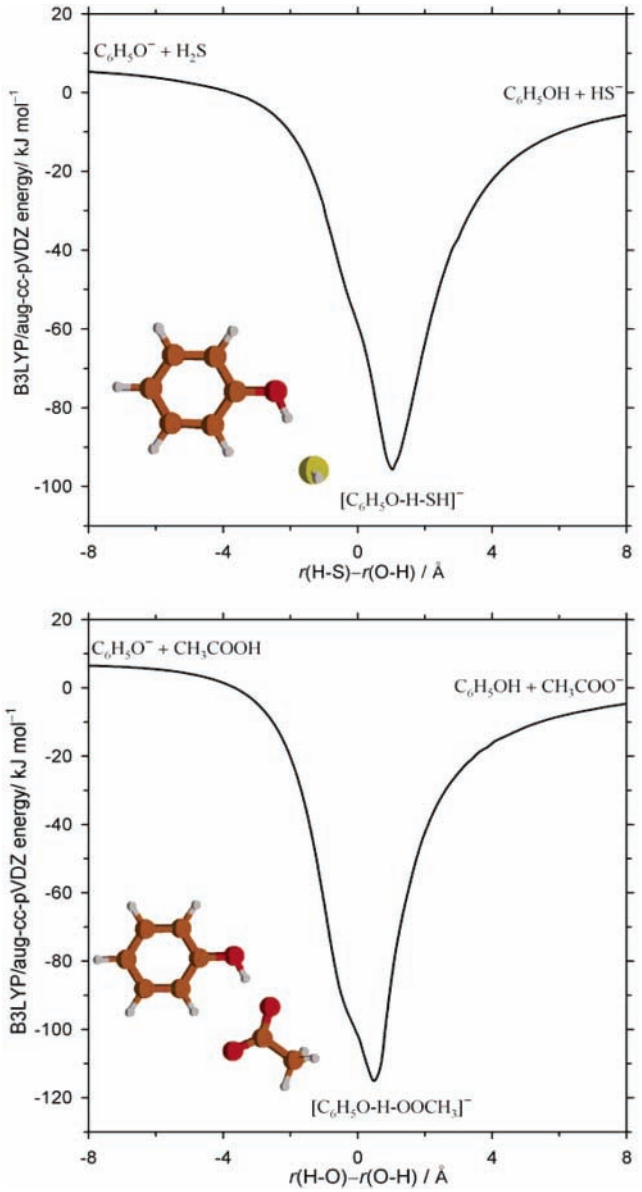

Figure 7. Potential energy surfaces for the dissociation of the $[C_6H_5O-H-SH]^-$ and $[C_6H_5O-H-OOCCH_3]^-$ anionic complexes in C_s symmetry. The energy relative to $HS^- + C_6H_5OH$ and $CH_3COO^- + C_6H_5OH$ is plotted versus the $r(H-S)-r(O-H)$ and $r(H-O)-r(O-H)$ distance, respectively, at the B3LYP/aug-cc-pVDZ level of theory without ZPE corrections.

is anchored to the absolute acidities of HCl or HF via a long chain of interlocking equilibrium measurements.[7] The HPMS work is similarly anchored via a long chain of interlocking equilibrium measurements to the gas-phase acidity of HCl.[10,80] In our TCID studies, the gas-phase acidity ladder is anchored by direct measurements to the anchor species of HCN, OOH, and H_2S, eliminating possible cumulative errors that could be present in the equilibrium studies.

Table 5 shows that the relative difference between the gas-phase acidities of $\Delta_{acid}H_{298}(C_6H_5OH)$ and $\Delta_{acid}H_{298}(3\text{-}CH_3C_6H_4OH)$ is a consistent $\delta\Delta_{acid}H_{298} = 1-2$ kJ/mol when compared within either the TCID, ICR, or HPMS experiments. However, the $\delta\Delta_{acid}H_{298} = +1$ to -7 kJ/mol between $\Delta_{acid}H_{298}(CH_3COOH)$ and $\Delta_{acid}H_{298}(C_6H_5OH)$ reveals an inconsistency. A contributor may be the entropy corrections used by NIST for the ICR and HPMS values which are derived from the original $\Delta_{acid}G_{380}$ and $\Delta_{acid}G_{600}$ measurements, respectively. The NIST temperature and entropy corrections are slightly different from the values calculated here from the harmonic frequencies and rotational constants shown in Table S1 with hindered-rotor treatments for torsions about the C−O axis. The greatest difference is for the entropy correction for $\Delta_{acid}H_{298}(CH_3COOH)$. NIST uses a ΔS_{298} value that increases the $\Delta_{acid}G_{298}$ value by 29−30 kJ/mol on conversion to $\Delta_{acid}H_{298}$, whereas our $\Delta S_{298} = 115 \pm 9$ J mol^{-1} K^{-1} increase it by 34 kJ/mol. If we use the experimental $S_{298}(CH_3COOH) = 282.84$ J mol^{-1} K^{-1} or experimental vibrational values for CH_3COOH from NIST,[58] the ΔS_{298} value increases further, resulting in an increase of 36 kJ/mol. An increase of 4−6 kJ/mol to the HPMS and ICR values for $\Delta_{acid}H_{298}(CH_3COOH)$ would give a better $\delta\Delta_{acid}H_{298}$ consistency within the separate experiments; although it would also make their absolute $\Delta_{acid}H_{298}(CH_3COOH)$ value move further away from our TCID $\Delta_{acid}H_{298}(CH_3COOH)$ result.

The HPMS study measured the $\delta\Delta_{acid}G_{600}$ directly between CH_3COOH and C_6H_5OH, and CH_3COOH and $3\text{-}CH_3C_6H_4OH$, providing $\delta\Delta_{acid}G_{600} = 6.7 \pm 1$ kJ/mol and $\delta\Delta_{acid}G_{600} = 7.9 \pm 1$ kJ/mol, respectively. These values compare reasonably well with our TCID $\delta\Delta_{acid}G_{298}$ values exhibited between CH_3COOH and C_6H_5OH, and CH_3COOH and $3\text{-}CH_3C_6H_4OH$, in Table 4. The ICR work also directly measured the $\delta\Delta_{acid}G_{380} = 1.7 \pm 1$ kJ/mol between C_6H_5OH and $3\text{-}CH_3C_6H_4OH$. This value is larger than our TCID value of $\delta\Delta_{acid}G_{298} = -1 \pm 7$ kJ/mol from Table 4.

In our previous paper,[23] we compared our derived O−H bond dissociation enthalpy of phenol, $D_{298}(C_6H_5O-H)$, with a selection of experimental and recommended values reported in the literature. Our refined value presented here, $D_{298}(C_6H_5O-H) = 361 \pm 4$ kJ/mol, is only 2 kJ/mol higher than our previous value and has not changed the context of that discussion. Table 6 compares our $D_{298}(C_6H_5O-H)$ value with an updated list of published $D_{298}(C_6H_5O-H)$ values from the literature. Our value has the best agreement with the recent reevaluation of the O−H bond dissociation enthalpy of phenol by Mulder et al.,[33] which recommends 363 ± 3 kJ/mol. The value recommended in the 2003 compilation by Luo,[32] $D_{298}(C_6H_5O-H) = 368 \pm 6$ kJ/mol, is also in reasonable agreement with our refined value with overlapping error bars. However, the 1998 evaluation by Borges dos Santos and Martinho Simões[30] recommended $D_{298}(C_6H_5O-H) = 371 \pm 2$ kJ/mol, which they derived from an average of seven values from gas-phase experiments that they considered to be the most reliable. Our refined value of $D_{298}(C_6H_5O-H) = 361 \pm 4$ kJ/mol supports a bond dissociation enthalpy that is significantly lower than this 1998 recommendation's value. Our value is also 16−20 kJ/mol lower than the two independent threshold values obtained from bimolecular proton-transfer reactions utilizing guided ion beam instruments: the mass-analyzed threshold ionization guided ion beam experiment (MATI/GIB) by Anderson and co-workers[22] who obtained $D_{298}(C_6H_5O-H) = 381 \pm 4$ kJ/mol from $C_6H_5OH^+ + ND_3$, and $D_{298}(C_6H_5O-H) = \leq 377 \pm 13$ kJ/mol obtained from $Cl^- + C_6H_5OH$ from this laboratory. As stated earlier, however, bimolecular proton-transfer reactions have been observed to give threshold energies that exceed the thermochemical value.[47] The proton-transfer reaction of $C_6H_5OH^+ + ND_3$ also includes competition from a dominant H/D exchange process. A large competitive shift and/or nonstatistical reaction dynamics due to the short-lived nature of a collision intermediate could cause the RRKM modeling used[22] to be unreliable for extracting the thermochemical threshold.

4.3. Comparison with Theory. Mulder et al.[33] in their recent reevaluation paper on the O−H bond dissociation enthalpy of phenol published G3, CBS-QB3, and CBS-APNO theoretical

TABLE 4: Final Recommended Thermochemical Values (kJ/mol)

species	$\Delta_{acid}H_0$	$\Delta_{acid}H_{298}$ [a]	$\Delta_{acid}S_{298}$ [b]	$\Delta_{acid}G_{298}$ [c]	D_0(RO−H)[d]	D_{298}(RO−H)[a]	Δ_fH_{298}(RO)[e]
C_6H_5OH	1451 ± 4	1456 ± 4	92 ± 6	1429 ± 4	356 ± 4	361 ± 4	47 ± 4
3-$CH_3C_6H_4OH$	1452 ± 5	1457 ± 5	97 ± 6	1428 ± 6	[351 ± 7[f]]	[356 ± 7]	[5 ± 7]
2,4,6-$(CH_3)_3C_6H_2OH$	1451 ± 4	1456 ± 4	105 ± 9	1425 ± 5	[334 ± 5[f]]	[340 ± 5]	[−55 ± 5]
CH_3COOH	1451 ± 6	1457 ± 6	115 ± 9	1422 ± 7	473 ± 6	479 ± 6	≥−171 ± 6

[a] Conversion to 298 K calculated by statistical mechanics in the independent-oscillator approximation using $\Delta_rH_{298} = \Delta_rH_0 + \int_0^{298}\Delta_rC_p(T)\,dT$ with harmonic frequencies and rotational constants shown in Table S1 except including hindered-rotor treatments for torsion about the C−O axis, and $H_{298} - H_0(H^+)$ and $H_{298} - H_0(H)$ from Gurvich et al.[52] [b] Gas-phase entropy (J mol^{-1} K^{-1}) calculated using the harmonic frequencies and rotational constants shown in Table S1 with hindered-rotor treatments for torsions about the C−O axis and $S_{298}(H^+)$ from Gurvich et al.[52] [c] $\Delta_{acid}G_{298} = \Delta_{acid}H_{298} - T\Delta_{acid}S_{298}$. [d] D_0(RO−H) = $\Delta_{acid}H_0$ + EA_0(RO) − IE_0(H). [e] Δ_fH_{298}(RO) = D_{298}(RO−H) + Δ_fH_{298}(ROH) − Δ_fH_{298}(H). [f] Values in brackets derived using EA_0(3-$CH_3C_6H_4O$) = 211.5 ± 4.0 kJ/mol and EA_0(2,4,6-$(CH_3)_3C_6H_2O$) = 195.1 ± 4.0 kJ/mol calculated at the CBS-QB3 level of theory with an uncertainty estimated from the absolute deviation of the CBS-QB3 value for $EA_0(C_6H_5O)$ = 215.1 kJ/mol and the experimental value.[19]

TABLE 5: Comparison of TCID $\Delta_{acid}H_{298}$ with NIST Recommended Literature Values (kJ/mol)

species	TCID[a]	ICR[b]	HPMS[c]
C_6H_5OH	1456 ± 4	1461 ± 9	1466 ± 10
3-$CH_3C_6H_4OH$	1457 ± 5	1463 ± 9	1467 ± 10
2,4,6-$(CH_3)_3C_6H_2OH$	1456 ± 4		
CH_3COOH	1457 ± 6	1459 ± 9	1459 ± 12
		1456 ± 9[d]	

[a] TCID, results derived from this work. [b] ICR, equilibrium study using an ion cyclotron resonance mass spectrometer.[7] [c] HPMS, equilibrium measurement using a high-pressure mass spectrometer.[10,80] [d] Reference 81.

TABLE 6: Comparison of the TCID Result with Recent Experimental Values (kJ/mol)

method[a]	year	$D_{298}(C_6H_5O-H)$	ref
TCID	2006	361 ± 4	this work
EVAL	2005	363 ± 3	33
TCID	2004	359 ± 8	23
EVAL	2003	368 ± 6	32
EVAL	1998	371 ± 2	30
MATI/GIB	2000	381 ± 4	22
PT/GIB	1998	≤377 ± 13	21

[a] TCID, results derived from this work and our previous publication;[23] EVAL, recommended value from reviews;[30,32,33] MATI/GIB, proton-transfer reaction using a guided ion beam with a mass-analyzed threshold ionization source;[22] PT/GIB proton-transfer reaction using a guided ion beam.[21]

TABLE 7: Comparison of TCID Results with Theory (kJ/mol)

method	$\Delta_{acid}H_{298}$ (C_6H_5OH)	D_{298} (C_6H_5O-H)	$\Delta_{acid}H_{298}$ (CH_3COOH)
TCID (this work)	1456 ± 4	361 ± 4	1457 ± 6
CCSD(T)/aug-cc-pVTZ[a,b]	1461		1456
B3LYP/aug-cc-pVTZ[a,b]	1456	351	1450
CBS-QB3[b−d]	1461	364	
G3//B3LYP[b,c]	1462	372	
G3[d]		369	
CBS-APNO[d]		369	
CCSD/cc-pVXZ[e]		373	

[a] At the geometry from the B3LYP/aug-cc-pVTZ level of theory. [b] Corrected with B3LYP/aug-cc-pVDZ zero point energy and converted to 298 K by statistical mechanics in the independent-oscillator approximation using $\Delta_rH_{298} = \Delta_rH_0 + \int_0^{298}\Delta_rC_p(T)\,dT$ with harmonic oscillator frequencies and rotational constants from Table S1 including hindered-rotor treatments for torsions about the C−O axis. [c] Reference 23. [d] Reference 33. [e] Basis-set extrapolated coupled cluster calculation, where X = D and T, calculated at the geometry optimization at the B3LYP/cc-pVTZ level of theory.[44]

$D_{298}(C_6H_5O-H)$ values, shown in Table 7. The G3 and CBS-APNO values both gave $D_{298}(C_6H_5O-H)$ = 369 kJ/mol, while CBS-QB3 gave $D_{298}(C_6H_5O-H)$ = 364 kJ/mol. The latter value agrees within the experimental uncertainties with both Mulder's reevaluated $D_{298}(C_6H_5O-H)$ = 363 ± 3 kJ/mol and our TCID value of $D_{298}(C_6H_5O-H)$ = 361 ± 4 kJ/mol. A recent theoretical paper by Costa Cabral and Canuto[44] presented a range of values for $D_{298}(C_6H_5O-H)$ using density functional theory and coupled cluster calculations and basis-set extrapolation methods. They concluded that a dual extrapolation of the CCSD/cc-pVDZ//B3LYP/cc-pVTZ and CCSD/cc-pVTZ//B3LYP/cc-pVTZ energies using the method of Truhlar[82] giving $D_{298}(C_6H_5O-H)$ = 373 kJ/mol is in good agreement with the Borges dos Santos and Martinho Simões[30] recommended value of $D_{298}(C_6H_5O-H)$ = 371 ± 2 kJ/mol and the earlier DeTuri and Ervin[21] value of $D_{298}(C_6H_5O-H) \le 377 \pm 13$ kJ/mol. However, as discussed earlier both these values are significantly higher than our newly recommended $D_{298}(C_6H_5O-H)$ = 361 ± 4 kJ/mol from the TCID method.

In our previous publication on phenol,[23] we used a selection of theoretical methods[76]—G3//B3LYP,[83,84] CBS-QB3,[85,86] and B3LYP/aug-cc-pVTZ[87−90]—to calculate the gas-phase acidity of phenol, the electron affinity of phenoxy radical, and the O−H bond dissociation energy of phenol. The theoretical values were found to be in better agreement among themselves for the gas-phase acidity of phenol (range of 6 kJ/mol) than for the electron affinity of phenoxy radical (range of 13 kJ/ mol) or the O−H bond dissociation energy of phenol (range of 21 kJ/mol). This reflects the difficulty of calculating energies for the open-shell aromatic phenoxy radical. DeTuri and Ervin[49] reported that higher-level methods, CCSD(T)/aug-cc-pVTZ//B3LYP/aug-cc-pVTZ or better, are required to obtain accurate gas-phase acidities within a few kilojoules per mole on the basis of an evaluation of 12 species that included benzene. Table 7 compares our TCID values of $\Delta_{acid}H_{298}(C_6H_5OH)$ and $\Delta_{acid}H_{298}(CH_3COOH)$ with those calculated at the CCSD(T)/aug-cc-pVTZ//B3LYP/aug-cc-pVTZ level of theory. The TCID measurement for $\Delta_{acid}H_{298}(CH_3COOH)$ is in good agreement with the CCSD(T)/aug-cc-pVTZ//B3LYP/aug-cc-pVTZ theoretical value. However, the TCID value for $\Delta_{acid}H_{298}(C_6H_5OH)$ is 5 kJ/mol lower than the CCSD(T)/aug-cc-pVTZ//B3LYP/aug-cc-pVTZ value and just outside the uncertainty of the TCID value. A full geometry optimization at the CCSD(T)/aug-cc-pVTZ level is beyond our current computational capability.

5. Conclusions

We have used the competitive threshold collision-induced dissociation method to obtain a local thermochemical network of gas-phase acidities. From this work, the gas-phase acidities of $\Delta_{acid}H_{298}(C_6H_5OH)$ = 1456 ± 4 kJ/mol, $\Delta_{acid}H_{298}$(3-$CH_3C_6H_4$-OH) = 1457 ± 5 kJ/mol, $\Delta_{acid}H_{298}$(2,4,6-$(CH_3)_3C_6H_2OH$) = 1456 ± 4 kJ/mol, and $\Delta_{acid}H_{298}(CH_3COOH)$ = 1457 ± 6 kJ/mol have been determined relative to the established literature values of hydrogen cyanide, hydrogen sulfide, and the hydro-

peroxyl radical. Our TCID value for $\Delta_{acid}H_{298}(CH_3COOH)$ agrees very well with the recommended value from NIST[58,81] and with theory at the CCSD(T)/aug-cc-pVTZ//B3LYP/aug-cc-pVTZ level. The TCID value for $\Delta_{acid}H_{298}(C_6H_5OH)$, however, is 5 kJ/mol lower than both the NIST recommended value[7,58] and the CCSD(T)/aug-cc-pVTZ//B3LYP/aug-cc-pVTZ theoretical value. Our TCID value for the O−H bond dissociation enthalpy of phenol, $D_{298}(C_6H_5O-H) = 361 \pm 4$ kJ/mol, is in good agreement with the recent reevaluation by Mulder et al.[33]

Acknowledgment. This research is supported by the U.S. Department of Energy, Office of Science, Office of Basic Energy Sciences, Chemical Sciences, Geosciences and Biosciences Division.

Supporting Information Available: Rotational constants, vibrational frequencies, polarizabilities, dipole moments, and rotational symmetries used in the RRKM models and for the thermal corrections (Table S1) and loose orbiting transition-state model fits for the $[RO-H-SH]^-$ data (Figure S1). This material is available free of charge via the Internet at http://pubs.acs.org.

References and Notes

(1) Rodgers, M. T.; Armentrout, P. B. *J. Chem. Phys.* **1998**, *109*, 1787.
(2) DeTuri, V. F.; Ervin, K. M. *J. Phys. Chem. A* **1999**, *103*, 6911.
(3) Ervin, K. M. *Chem. Rev.* **2001**, *101*, 391.
(4) Bartmess, J. E. Negative Ion Energetics Data. In *NIST Chemistry WebBook*; Mallard, W. G., Linstrom, P. J., Eds.; NIST Standard Reference Database Number 69; National Institute of Standards and Technology: Gaithersburg, MD, 2005 (Jun). (http://webbook.nist.gov).
(5) Bartmess, J. E. *Mass Spectrom. Rev.* **1989**, *8*, 297.
(6) Bartmess, J. E.; Scott, J. A.; McIver, R. T., Jr. *J. Am. Chem. Soc.* **1979**, *101*, 6046.
(7) Fujio, M.; McIver, R. T., Jr.; Taft, R. W. *J. Am. Chem. Soc.* **1981**, *103*, 4017.
(8) Paul, S.; Back, M. H. *Can. J. Chem.* **1975**, *53*, 3330.
(9) Colussi, A. J.; Zabel, F.; Benson, S. W. *Int. J. Chem. Kinet.* **1977**, *9*, 161.
(10) Cumming, J. B.; Kebarle, P. *Can. J. Chem.* **1978**, *56*, 1.
(11) DeFrees, D. J.; McIver, R. T., Jr.; Hehre, W. J. *J. Am. Chem. Soc.* **1980**, *102*, 3334.
(12) Peters, K. S. *Pure Appl. Chem.* **1986**, *58*, 1263.
(13) Lin, C.-Y.; Lin, M. *J. Phys. Chem.* **1986**, *90*, 425.
(14) Arends, I.; Louw, R.; Mulder, P. *J. Phys. Chem.* **1993**, *97*, 7914.
(15) Bordwell, F. G.; Cheng, J.-P.; Harrelson, J. A., Jr. *J. Am. Chem. Soc.* **1988**, *110*, 1229.
(16) Mackie, J.; Doolan, K.; Nelson, P. *J. Phys. Chem.* **1989**, *93*, 664.
(17) Suryan, M. M.; Kafafi, S. A.; Stein, S. E. *J. Am. Chem. Soc.* **1989**, *111*, 1423.
(18) Walker, J. A.; Tsang, W. *J. Phys. Chem.* **1990**, *94*, 3324.
(19) Gunion, R. F.; Gilles, M. K.; Polak, M. L.; Lineberger, W. C. *Int. J. Mass Spectrom. Ion Processes* **1992**, *117*, 601.
(20) Hoke, S. H., II.; Yang, S. S.; Cooks, R. G. *J. Am. Chem. Soc.* **1994**, *116*, 4888.
(21) DeTuri, V. F.; Ervin, K. M. *Int. J. Mass Spectrom.* **1998**, *175*, 123.
(22) Kim, H.-T.; Green, R. J.; Qian, J.; Anderson, S. L. *J. Chem. Phys.* **2000**, *112*, 5717.
(23) Angel, L. A.; Ervin, K. M. *J. Phys. Chem. A* **2004**, *108*, 8346.
(24) Wayner, D. D. M.; Lusztyk, E.; Page D.; Ingold, K. U.; Mulder, P.; Laarhoven, L. J. J.; Aldrich, H. S. *J. Am. Chem. Soc.* **1995**, *117*, 8737.
(25) Guedes, R.; Coutinho; Cabral, B.; Canuto, S.; Correia, C. F.; Borges dos Santos, R. M.; Martinho Simoes, J. *J. Phys. Chem. A* **2003**, *107*, 9197.
(26) Correia, C. F.; Nunes, P. M.; Borges dos Santos, R. M.; Martinho Simoes, J. *Thermochim. Acta* **2004**, *420*, 3.
(27) McMillen, D. F.; Golden, D. M. *Annu. Rev. Phys. Chem.* **1982**, *33*, 493.
(28) Back, M. H. *J. Phys. Chem.* **1989**, *93*, 6880.
(29) Tsang, W. In *Energetics of Organic Free Radicals*; Simões, J. A., Greenberg, A., Liebman, J. F., Eds.; Blackie Academic and Professional: London, 1996; p 22.
(30) Borges dos Santos, R. M.; Martinho Simoes, J. A. *J. Phys. Chem. Ref. Data* **1998**, *27*, 707.
(31) Blanksby, S. J.; Ellison, G. B. *Acc. Chem. Res.* **2003**, *36*, 255.
(32) Luo, Y.-R. *Handbook of Bond Dissociation Energies in Organic Compounds*; CRC Press: Boca Raton, FL, 2003.
(33) Mulder, P.; Korth, H.-G.; Pratt, D. A.; DiLabio, G. A.; Valgimigli, L.; Pedulli, G. F.; Ingold, K. U. *J. Phys. Chem. A* **2005**, *109*, 2647.
(34) Wright J. S.; Carpenter, D. J.; McKay, D. J.; Ingold, K. U. *J. Am. Chem. Soc.* **1997**, *119*, 4245.
(35) DiLabio, G. A.; Pratt, D. A.; LoFaro, A. D.; Wright J. S. *J. Phys. Chem. A* **1999**, *103*, 1653.
(36) Guedes, R.; Cabral, B.; Martinho Simoes, J.; Diogo, H. *J. Phys. Chem. A* **2000**, *104*, 6062.
(37) Couto, P.; Guedes, R.; Cabral, B.; Martinho Simoes, J. *Int. J. Quantum Chem.* **2002**, *86*, 297.
(38) Johnson, E. R.; Clarkin, O. J. D., G. A. *J. Phys. Chem. A* **2003**, *107*, 9953.
(39) Bakalbassis, E. G.; Lithoxoidu, A. T.; Vafiadis, A. P. *J. Phys. Chem. A* **2003**, *107*, 8594.
(40) Estacio, S. G.; Couto, P.; Guedes, R.; Cabral, B.; Martinho Simoes, J. *Theor. Chem. Acc.* **2004**, *112*, 282.
(41) Busch, M. S.; Knapp, E.-W. *ChemPhysChem* **2004**, *5*, 1513.
(42) Guerra, M.; Amorati, R.; Pedulli, G. F. *J. Org. Chem.* **2004**, *69*, 5460.
(43) Wright, J. S.; Rowley, C. N.; Chepelev, L. L. *Mol. Phys.* **2005**, *103* (6−8), 815.
(44) Costa Cabral, B. J.; Canuto, S. *Chem. Phys. Lett.* **2005**, *406*, 300.
(45) DiLabio, G. A.; Mulder, P. *Chem. Phys. Lett.* **2006**, *417*, 566.
(46) Costa Cabral, B. J.; Canuto, S. *Chem. Phys. Lett.* **2006**, *417*, 570.
(47) DeTuri, V. F.; Su, M. A.; Ervin, K. M. *J. Phys. Chem. A* **1999**, *103*, 1468.
(48) Rodgers, M. T.; Ervin, K. M.; Armentrout, P. B. *J. Chem. Phys.* **1997**, *106*, 4499.
(49) DeTuri, V. F.; Ervin, K. M. *J. Phys. Chem. A* **2002**, *106*, 9947.
(50) Bradforth, S.; Kim, E.; Arnold, D.; Neumark, D. *J. Chem. Phys.* **1993**, *98*, 800.
(51) Cook, P. A.; Langford, S. R.; Ashfold, M. N. R.; Dixon, R. N. *J. Chem. Phys.* **2000**, *113*, 994.
(52) Gurvich, L. V.; Veyts, I. V.; Alcock, C. B. *Thermodynamic Properties of Individual Substances*, 4th ed.; Hemisphere: New York, 1989; Vol. 1 (Elements O, H (D, T), F, Cl, Br, I, He, Ne, Ar, Kr, Xe, Rn, S, N, P and Their Compounds), Parts 1−2.
(53) Ervin, K. M.; Anusiewicz, I.; Skurski, P.; Simons, J.; Lineberger, C. W. *J. Phys. Chem. A* **2003**, *107*, 8521.
(54) Litorja, M.; Ruscic, B. *J. Electron Spectrosc. Relat. Phenom.* **1998**, *97*, 131.
(55) Ramond, T. M.; Blanksby, S. J.; Kato, S.; Bierbaum, V. M.; Davico, G. E.; Schwartz, R. L.; Lineberger, W. C.; Ellison, G. B. *J. Phys. Chem. A* **2002**, *106*, 9641.
(56) Shiell, R. C.; Hu, X. K.; Hu, Q. J.; Hepburn, J. W. *J. Phys. Chem. A* **2000**, *104*, 4339.
(57) Pedley, J. B. *Thermochemical Data and Structures of Organic Compounds*; TRC Data Series; Thermodynamics Research Center: College Station, TX, 1994; Vol. 1.
(58) *NIST Chemistry WebBook*; Linstrom, P. J., Mallard, W. G., Eds.; NIST Standard Reference Database Number 69; National Institute of Standards and Technology: Gaithersburg, MD, 2005 (Jun).
(59) Cox, J. *Pure Appl. Chem.* **1961**, *2*, 125.
(60) Lias, S. G.; Bartmess, J. E.; Liebman, J. F.; Holmes, J. L.; Levin, R. D.; Mallard, W. G. *J. Phys. Chem. Ref. Data* **1988**, *17* (Suppl. 1).
(61) Lu, Z.; Continetti, R. E. *J. Phys. Chem. A* **2004**, *108*, 9962.
(62) DeTuri, V. F.; Hintz, P. A.; Ervin, K. M. *J. Phys. Chem. A* **1997**, *101*, 5969.
(63) Angel, L. A.; Ervin, K. M. *J. Am. Chem. Soc.* **2003**, *125*, 1014.
(64) Ervin, K. M.; Armentrout, P. B. *J. Chem. Phys.* **1985**, *83*, 166.
(65) Armentrout, P. B.; Ervin, K. M. CRUNCH, Fortran program, version 5.0, 2002.
(66) Baer, T.; Hase, W. L. *Unimolecular Reaction Dynamics: Theory and Experiments*; Oxford University Press: New York, 1996.
(67) Gilbert, R. G.; Smith, S. C. *Theory of Unimolecular and Recombination Reactions*; Blackwell Scientific: Boston, 1990.
(68) Iceman, C.; Armentrout, P. *Int. J. Mass Spectrom.* **2003**, *222*, 329.
(69) Miller, T. M. Atomic and Molecular Polarizabilities. In *Handbook of Chemistry and Physics*, 83rd ed.; Lide, D. R., Ed.; CRC Press: Boca Raton, FL, 2002; p 163.
(70) Dipole Moments. In *Handbook of Chemistry and Physics*; 83rd ed.; Lide, D. R., Ed.; CRC Press: Boca Raton, FL, 2002; p 45.
(71) Chesnavich, W. J.; Bass, L.; Su, T.; Bowers, M. T. *J. Chem. Phys.* **1981**, *74*, 2228.
(72) Muntean, F.; Armentrout, P. B. *J. Chem. Phys.* **2001**, *115*, 1213.
(73) Chantry, P. J. *J. Chem. Phys.* **1971**, *55*, 2746.
(74) Lifshitz, C.; Wu, R.; Tiernan, T.; Terwilleger, D. *J. Chem. Phys.* **1978**, *68*, 247.
(75) Taylor, B. N.; Kuyatt, C. *Guidelines for Evaluating and Expressing the Uncertainty of NIST Measurement Results*; NIST Technical Note 1297; National Institute of Standards and Technology: Washington, DC, 1994.

(76) Frisch, M. J.; Trucks, G. W.; Schlegel, H. B.; Scuseria, G. E.; Robb, M. A.; Cheeseman, J. R.; Montgomery, J. A., Jr.; Vreven, T.; Kudin, K. N.; Burant, J. C.; Millam, J. M.; Iyengar, S. S.; Tomasi, J.; Barone, V.; Mennucci, B.; Cossi, M.; Scalmani, G.; Rega, N.; Petersson, G. A.; Nakatsuji, H.; Hada, M.; Ehara, M.; Toyota, K.; Fukuda, R.; Hasegawa, J.; Ishida, M.; Nakajima, T.; Honda, Y.; Kitao, O.; Nakai, H.; Klene, M.; Li, X.; Knox, J. E.; Hratchian, H. P.; Cross, J. B.; Adamo, C.; Jaramillo, J.; Gomperts, R.; Stratmann, R. E.; Yazyev, O.; Austin, A. J.; Cammi, R.; Pomelli, C.; Ochterski, J. W.; Ayala, P. Y.; Morokuma, K.; Voth, G. A.; Salvador, P.; Dannenberg, J. J.; Zakrzewski, V. G.; Dapprich, S.; Daniels, A. D.; Strain, M. C.; Farkas, O.; Malick, D. K.; Rabuck, A. D.; Raghavachari, K.; Foresman, J. B.; Ortiz, J. V.; Cui, Q.; Baboul, A. G.; Clifford, S.; Cioslowski, J.; Stefanov, B. B.; Liu, G.; Liashenko, A.; Piskorz, P.; Komaromi, I.; Martin, R. L.; Fox, D. J.; Keith, T.; Al-Laham, M. A.; Peng, C. Y.; Nanayakkara, A.; Challacombe, M.; Gill, P. M. W.; Johnson, B.; Chen, W.; Wong, M. W.; Gonzalez, C.; Pople, J. A. *Gaussian 03*, Revision C.02; Gaussian, Inc.: Pittsburgh, PA, 2004.

(77) Ruscic, B.; Pinzon, R. E.; Morton, M. L.; Laszevski, G. v.; Bittner, S. J.; Nijsure, S. J.; Amin, K. A.; Minkoff, M.; Wagner, A. F. *J. Phys. Chem. A* **2004**, *108*, 9979.

(78) Skoog, D. A.; West, D. M.; Holler, F. J. *Analytical Chemistry: An Introduction*, 6th ed.; Saunders College Publishing: Philadelphia, 1994; p 91.

(79) F. A. Akin; K. M. Ervin. *J. Phys. Chem. A* **2006**, *110*, 1342.

(80) Kebarle, P.; McMahon, T. B. *J. Am. Chem. Soc.* **1977**, *99*, 2222.

(81) Taft, R. W.; Topsom, R. D. *Prog. Phys. Org. Chem.* **1987**, *16*, 1.

(82) Truhlar, D. G. *Chem. Phys. Lett.* **1998**, *294*, 45.

(83) Curtiss, L. A.; Raghavachari, K.; Redfern, P. C.; Rassolov, V.; Pople, J. A. *J. Chem. Phys.* **1998**, *109*, 7764.

(84) Baboul, A. G.; Curtiss, L. A.; Redfern, P. C.; Raghavachari, K. *J. Chem. Phys.* **1999**, *110*, 7650.

(85) Jursic, B. S. *J. Mol. Struct. (THEOCHEM)* **2000**, *498*, 123.

(86) Pokon, E. K.; Liptak, M. D.; Feldgus, S.; Shields, G. C. *J. Phys. Chem. A* **2001**, *105*, 10483.

(87) Becke, A. *J. Chem. Phys.* **1993**, *98*, 5648.

(88) Dunning, T. H., Jr. *J. Chem. Phys.* **1989**, *90*, 1007.

(89) Kendall, R. A.; Dunning, T. H., Jr.; Harrison, R. J. *J. Chem. Phys.* **1992**, *96*, 6792.

(90) Woon, D. E.; Dunning, T. H., Jr. *J. Chem. Phys.* **1993**, *98*, 1358.